Heliyon 10 (2024) e39861

Contents lists available at ScienceDirect

Heliyon

journal homepage: www.cell.com/heliyon

Research article

# Pan-cancer analysis of IRF1 focusing on prognostic and immunological roles in non-small cell lung cancer

Weiling Sun [a,b,1], Kui Cao [c,1], Siran Wang [d,1], Mengdi Lu [c], Jianqun Ma [c,**], Chunlong Wu [b,***], Yanbin Zhao [a,*]

[a] Department of Medical Oncology, Harbin Medical University Cancer Hospital, 150 Haping Road, Harbin, 150040, China
[b] Department of Endoscope, Harbin Medical University Cancer Hospital, 150 Haping Road, Harbin, 150040, China
[c] Department of Thoracic Surgery, Harbin Medical University Cancer Hospital, 150 Haping Road, Harbin, 150040, China
[d] Department of Preventive Dentistry, Guangdong Engineering Research Center of Oral Restoration and Reconstruction, Guangzhou Key Laboratory of Basic and Applied Research of Oral Regenerative Medicine, Affiliated Stomatology Hospital of Guangzhou Medical University, 510182, Guangzhou, China

ARTICLE INFO

*Keywords:*
Pan-cancer
IRF1
NSCLC
Prognosis
Tumour microenvironment
Immune-related genes

ABSTRACT

Interferon regulatory factor 1 (IRF1) significantly affects tumour occurrence and development. This study aimed to analyse its function as a pan-cancer prognostic indicator. We compared IRF1 expression and prognostic significance in normal and tumour samples from different databases. Accordingly, we performed *in vitro* experiments and immunohistochemistry (IHC) to investigate the role of IRF1 in non-small cell lung cancer (NSCLC). Our findings indicate that IRF1 expression is significantly correlated with prognosis, the tumour microenvironment, and immune cell infiltration. Furthermore, receiver operating characteristic (ROC) analysis revealed that IRF1 had high accuracy in distinguishing cancerous tissues from normal ones. Notably, IRF1 expression was linked to immune-related and immune checkpoint genes. Cell proliferation, invasion, and migration were significantly related to IRF1 expression. IHC indicated that IRF1 was downregulated in NSCLC tissues. Our study provides comprehensive bioinformatic analysis and experimental verification of IRF1, suggesting its potential as a prognostic biomarker in cancer.

## 1. Introduction

Interferon regulatory factor 1 (IRF1), part of the interferon regulatory factor family, is recognized as a nuclear transcription factor that plays critical roles in the regulation of interferon expression [1], as well as in both innate and adaptive immunity [2], and has an anti-oncogenic latent role in some malignant diseases [3], including leukaemia [4], gastric cancer (GC) [5], and other carcinomas.

Several studies suggested that IRF1 mediates apoptosis [6] and autophagy [7] in breast cancer cells. IRF1 can reverse multiple drug resistance by decreasing P-glycoprotein expression [8] and inhibiting its effect on chemotherapy resistance in GC. IRF1 could mediate IFN-γ-induced apoptosis via regulation of caspase-1 or caspase-8 expression to sensitise cells to apoptosis in ovarian cancer cell lines.

* Corresponding author. Department of Medical Oncology, Harbin Medical University Cancer Hospital, 150 Haping Road, Harbin, 150040, China.
** Corresponding author.
*** Corresponding author.
*E-mail addresses:* jianqunma@hrbmu.edu.cn (J. Ma), wuchunlong1968@aliyun.com (C. Wu), zhaoyanbin1978@sina.com (Y. Zhao).
[1] These authors contributed equally to this work.

https://doi.org/10.1016/j.heliyon.2024.e39861
Received 25 May 2023; Received in revised form 17 October 2024; Accepted 25 October 2024
Available online 7 November 2024

IRF1 could help prevent colorectal cancer by modulating apoptosis, pyroptosis and necroptosis (PANoptosis) [9].

Immune checkpoint blockade (ICB) targeting programmed death-1 (PD-1)/programmed death ligand-1 (PD-L1) has shown remarkable promise in immunotherapy [10–12]. However, some patients are insensitive to PD1/PD-L1 inhibitors [13,14]. Identifying a novel therapeutic target to address the limitations of PD-1/PD-L1 antibodies presents a promising strategy for minimizing the recurrence of advanced cancer. IRF1 is required for DSB-dependent PD-L1 upregulation [15]. IRF1 is capable of binding to the PD-L1 promoter, thereby enhancing PD-L1 transcription in melanoma cells [16] and participate in the activation of PD-L1 mRNA synthesis at the transcriptional level in osteosarcoma (OS), lung adenocarcinoma (LUAD), prostate cancer (PCA) and hepatocellular carcinoma (HCC) [17,18].

Furthermore, the tumour microenvironment (TME) is composed of diverse cellular components and an extracellular matrix, along with infiltrating immune cells constituting a significant portion [19]. These immune cells are essential to cancer progression [20]. The TME encompasses numerous cellular elements and surrounding matrix constituents that are intimately associated with tumour escape, progression, and therapeutic responses [21,22]. Recent studies have shown that IRF1 contributes to the antitumour microenvironment in HCC [23].

This study evaluated the clinical importance and prognostic usefulness of IRF1 across different types of cancer. We used The Cancer Genome Atlas (TCGA) and the Genotype-Tissue Expression (GTEx) databases to analyse IRF1 expression in normal and tumour tissues. We also examined the association between IRF1 expression and tumour clinical stage, tumour immune cell infiltration, tumour mutational burden (TMB), and microsatellite instability (MSI) using multiple databases. Our findings demonstrate the prognostic significance of IRF1 across various cancer types. Thus, IRF1 may have excellent potential as a therapeutic target for predicting the efficacy of immunotherapy. We also conducted experimental validation of IRF1's role in NSCLC to evaluate its potential as a predictive biomarker for prognosis.

## 2. Methods

### 2.1. Data collection

We downloaded RNA sequencing expression data and clinicopathological information for 33 distinct tumours from TCGA database (https://portal.gdc.cancer.gov/), GTEx datasets (https://www.gtexportal.org/) and the Gene Expression Omnibus (GEO) database (http://www.ncbi.nih.gov/geo/). Using Gene Expression Profiling Interactive Analysis (GEPIA) (http://gepia.cancer-pku.cn/) [24], we compared IRF1 expression levels between tumour and normal tissues. This analysis utilized gene expression data from TCGA and various normal tissues sourced from the GTEx database (https://www.genome.gov/Funded-Programs-Projects/Genotype-Tissue-Expression-Project). Protein expression levels of IRF1 in primary tumours versus normal tissues were investigated through the University of Alabama at Birmingham Cancer Data Analysis Portal (UALCAN) database (http://ualcan.path.uab.edu/analysis-prot.html) [25], with data obtained from the Clinical Proteomic Tumour Analysis Consortium (CPTAC). Additionally, IRF1 expression across different tumour stages within TCGA using GEPIA. Finally, single-cell level expression data for IRF1 across various tumours were obtained from the Tumour Immune Single-cell Hub 2 (TISCH2).

### 2.2. Survival analysis

We investigated the association between levels of IRF1 expression and long-term survival outcomes in cancer, applying data from the TCGA database. We extracted clinical variables, including overall survival (OS), disease-specific survival (DSS), progression-free interval (PFI), and disease-free interval (DFI) from TCGA and the Kaplan–Meier (KM) Plotter. Patients were classified into $IRF1^{high}$ and $IRF1^{low}$ groups according to the minimum *p*-value method. Kaplan–Meier survival curves and forest plots from univariate Cox regression analyses of IRF1 were generated using the R packages "survival", "survminer", and "forestplot".

### 2.3. Prognostic capacity of IRF1 to differentiate tumour from non-tumour tissues

We conducted a ROC analysis to assess the ability of IRF1 expression levels to distinguish tumour tissues from normal tissues across 33 cancer types, utilizing the "pROC" R package. The area under the curve (AUC) was calculated, with values exceeding 0.7 deemed significantly acceptable.

### 2.4. Correlation analysis of IRF1 with TMB, MSI, and immune cell infiltration

Somatic mutation data for cancer patients were obtained from the TCGA database (https://tcga.xenahubs.net), from which we calculated TMB scores for each sample using the "maftools" R package. MSI scores for the tumours were sourced from published literature. To evaluate the correlation among IRF1, TMB, and MSI, we employed the Spearman's rank correlation method, with results visualized using radar charts. Furthermore, we adopted single-sample GSEA (ssGSEA) to assess immune cell types from different expression levels of IRF1 in 24 immune cell subpopulations and different amounts of tumour-infiltrating immune cells in NSCLC established previously.

### 2.5. Immune analysis

The levels of estimated stromal and immune cells in cancerous tissues were compared by computing the StromalScore and ImmuneScore utilizing the Estimation of Stromal and Immune cells in Malignant Tumour tissues using Expression data (ESTIMATE) method (https://bioinformatics.mdanderson.org/estimate/disease.html). Gene sets were sourced from the HALLMARK, Gene Ontology (GO), and Kyoto Encyclopedia of Genes and Genomes (KEGG) pathway databases. Spearman correlations were also conducted to determine correlation heatmaps of IRF1 with immunomodulators (immune suppressive genes, immune activation genes, major histocompatibility complex (MHC) genes, chemokines, and chemokine receptor genes), and p-values were generated without adjustments. Additionally, Pearson's correlation analyses were executed to explore the association between IRF1 expression and genes relevant to immune infiltration and immune checkpoints.

### 2.6. Cell culture and transfection

Human lung bronchial epithelial cells (Beas-2B) and four human NSCLC cell lines (H292, H460, PC9 and H1993) were obtained from the Cell Bank of the Chinese Academy of Sciences (Shanghai, China). Beas-2B and PC9 cells were cultured in Dulbecco's Modified Eagle Medium (DMEM, Gibco, Life Technologies, California, USA), while H292, H460 and H1993 cells were maintained in RPMI-1640 medium (Gibco, California, USA) supplemented with 10 % fetal bovine serum (PAN-Biotech, Aidenbach, Germany), penicillin G (100 U/mL, Beyotime, China), and streptomycin (10,000 μg/mL, Sevenbio, Beijing, China). All cell lines were incubated in a humidified atmosphere at 37 °C with 5 % $CO_2$.

For functional analysis, cells were transfected with lentiviruses containing sequences for overexpression or knockdown of IRF1, sourced from KeyGen BioTECH (Nanjing, China), and selected using puromycin. The specific target sequences are detailed in Table S1.

### 2.7. Single-cell gene expression heterogeneity analysis between IRF1-high and IRF1-low cancer cells

A single-cell Seurat object was constructed utilizing the Seurat R package. After quality control, standardisation, PCA, and UMAP dimensionality reduction, cells were classified according to the expression of various cell-type marker genes (filled in by the cells on the graph). Malignant epithelial cells were then extracted for dimensionality reduction analysis, and malignant epithelial cells were grouped into high and low IRF1 expression categories according to their IRF1 expression levels. To identify differentially expressed genes correlated with IRF1, volcano plots were generated utilizing the ggplot2 library in R. To explore the roles and relationships of IRF1, GO analysis for biological processes and KEGG for differential genes were applied.

### 2.8. Western blot (WB) and quantitative real PCR (qRT-PCR)

Cells were collected and subsequently washed twice with phosphate-buffered saline (PBS, Sevenbio, Beijing, China), then lysed on ice at 4 °C using RIPA buffer (Sevenbio, Beijing, China) supplemented with a proteinase inhibitor cocktail (Sevenbio, Beijing, China) for 20 min. Equal quantities of protein were separated by SDS-PAGE (10 %) and subsequently transferred onto polyvinylidene fluoride (PVDF) membranes. Then the membranes were blocked with 5 % skimmed milk in PBST at room temperature for 2 h. They were incubated overnight at 4 °C with primary antibodies against IRF1 (1:1000, Abcam, #ab191032), β-ACTIN (1:1000, ZSGB-BIO, #TA-09) and GAPDH (1:5000, Abcam, #ab8245), as indicated in Table S2. Following washing with PBST, the membranes were treated with horseradish peroxidase (HRP)-conjugated secondary antibodies (1:1000; Zhongshan Golden Bridge Biotechnology Co., Ltd., Beijing, China) for 1 h at room temperature. The target protein bands were detected using an ECL detection system (Proteintech).

The E.Z.N.A. Total RNA Kit I (R6834-01, Omega Bio-Tek, United States) was used to extract RNA from the cells. Complementary DNA was synthesized with a high-capacity cDNA reverse transcription kit. qRT-PCR was performed with the Applied Biosystems StepOne Real-Time PCR System employing FastStart Universal SYBR Green Master (Roche, Mannheim, Germany), with GAPDH serving as the internal control.

Primers were as follows:

5′-CTCTCACCAAGAACCAGAGAAA-3′ (forward) and 5′-GAAGGTATCAGGGCTGGAATC-3′ (reverse) for IRF1;

5′-CATGTTCGTCATGGGTGTGAA-3′ (forward) and 5′-GGCATGGACTGTGGTCATGAG-3′ (reverse) for GAPDH.

### 2.9. Cell viability

For the Cell Counting Kit-8 (CCK8) assay, $4 \times 10^3$ cells were plated in each well of a 96-well plate. At specified time points (1, 2, 3, and 4 days, as well as 24, 48, 72, and 96 h), the cells were incubated with 10 μL of CCK-8 reagent (Meilunbio, Dalian, China) for 2 h at 37 °C. The optical density (OD) was subsequently measured at 450 nm.

### 2.10. Transwell and wound healing assays

In the transwell assays, a defined number of cells ($4 \times 10^4$ cells per well for migration and $8 \times 10^4$ cells per well for invasion) were suspended in 200 μL of serum-free medium and added to the upper inserts, either with or without Matrigel (BD Biosciences, San Jose, CA, USA). Following incubation for 24–72 h (24 h for migration and 72 h for invasion), the cells that migrated to the bottom surface were fixed using 4 % paraformaldehyde and subsequently stained with 0.1 % crystal violet. Five randomly selected visual fields from

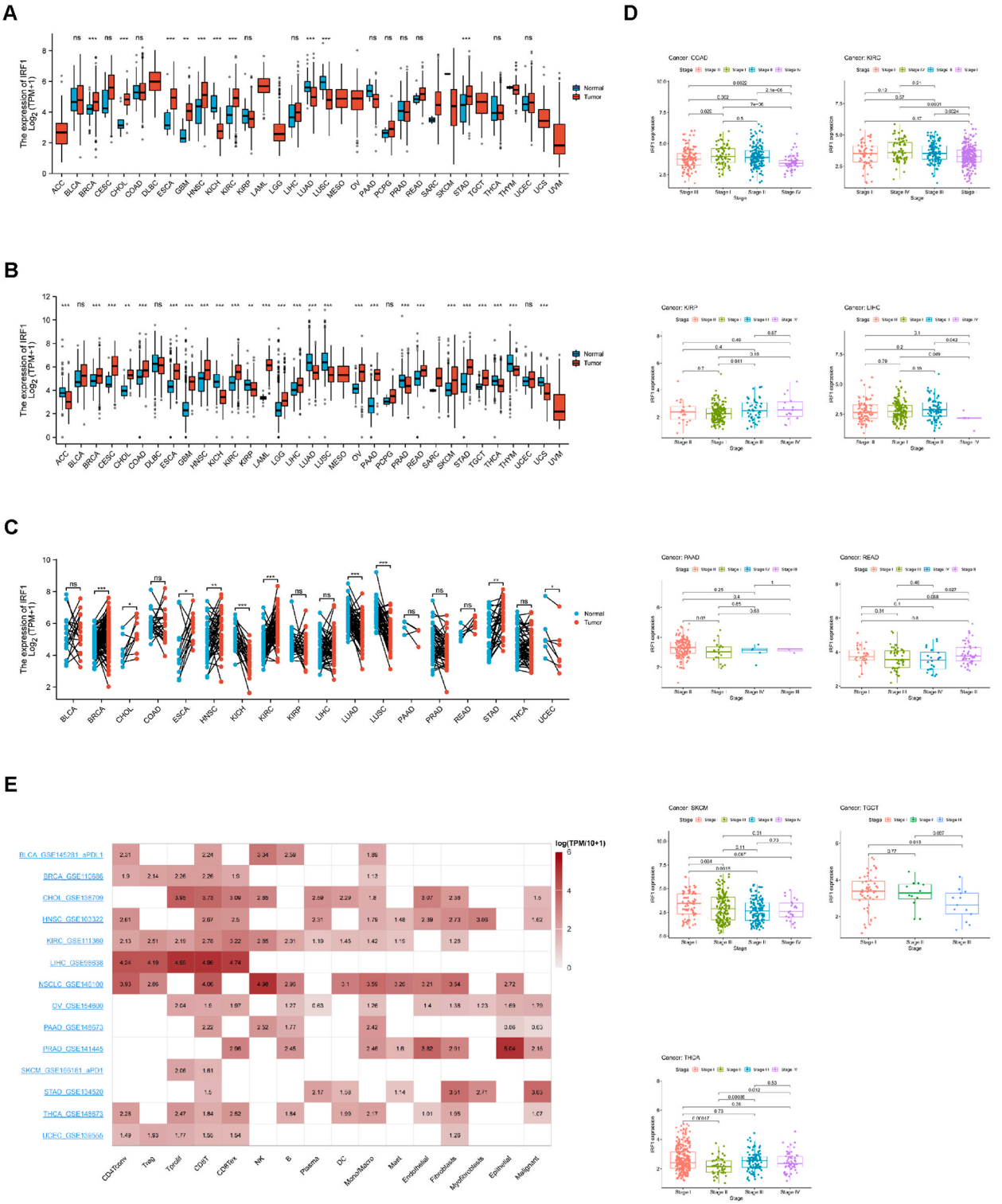


**Fig. 1.** The expression levels of IRF1 across various cancers, normal tissues, and different pathological stages. (A) Differential expression of IRF1 was analyzed in pan-cancer tissues derived from TCGA datasets. (B) The differential expression of IRF1 across pan-cancer tissues using both TCGA and GTEx datasets. (C) IRF1 expression in paired cancer tissues and adjacent normal tissues sourced from TCGA. (D) Using TCGA data, the expression levels of the IRF1 gene across stages I, II, III, and IV. (E) Single-cell expression patterns of IRF1 in a pan-cancer context. Log2 (TPM + 1) was applied for the log scale. *$p < 0.05$; **$p < 0.01$; ***$p < 0.001$; ****$p < 0.0001$.

each insert were photographed, and the cell count was determined manually. In the wound healing assays, artificial wounds were created on a monolayer of cells by scratching across the center of the well with 10 μL pipette tips until the cells covered 95 % of the surface of the 6-well plate. Images of wound healing were captured at 0 and 48 h.

### 2.11. Patient information and tissue specimens

Paraffin-embedded samples were collected from 187 patients (115 LUAD tissues, 72 lung squamous cell carcinoma (LUSC) tissues, and 31 normal lung tissues) who were treated with surgical removal or underwent CT- or bronchoscopy-guided pathological biopsy between January 2011 and December 2015, with follow-up until December 2019 at Harbin Medical University Cancer Hospital. OS and PFS were calculated as the interval from surgery or pathological biopsy to death or relapse, respectively. Notably, none of the patients had received radiotherapy or chemotherapy prior to surgery or biopsy. Comprehensive clinicopathological and follow-up data were also gathered (Table S3). The use of human tissues was approved by the Institutional Research Ethics Committee of Harbin Medical University Cancer Hospital. All participants provided the written informed consent.

### 2.12. Immunohistochemistry (IHC)

Paraffin-embedded tissue specimens were sectioned and deparaffinized in xylene, followed by rehydration and antigen retrieval using ethylenediaminetetraacetic acid (EDTA). Immunohistochemical staining was performed using the IRF1 primary antibody (1:1000; Abcam, #ab191032) (Table S2) overnight at 4 °C. Then it was incubated with horseradish peroxidase (HRP)-labeled secondary antibody (ZSGB-BIO, PV6001) Immunohistochemical staining was conducted using an IRF1 primary antibody (1:1000; Abcam, #ab191032) (Table S2) and incubated overnight at 4 °C. Following this, the specimens were exposed to a horseradish peroxidase (HRP)-labeled secondary antibody (ZSGB-BIO, PV6001). Staining was subsequently performed using a DAB kit (ZSGB-BIO, ZLI-9019) until the desired staining intensity was reached. Following staining, sections were counterstained with haematoxylin, dehydrated, and covered with coverslips.

Staining results were examined independently by two blinded observers using predefined criteria. The percentage of positively stained cells was scored as follows: 0 (0%–5%), 1 (6%–25 %), 2 (26%–50 %), 3 (51%–75 %), and 4 (76%–100 %). Staining intensity was classified as 0 (no staining), 1 (weak and incomplete), 2 (moderate to complete), or 3 (strong and complete). The final IRF1 expression score was derived by multiplying the percentage of positively stained cells by the corresponding intensity score. For statistical analysis, a final staining score of 7 or higher was classified as indicative of high expression, whereas a score smaller than 7 as a low expression.

### 2.13. In vivo assay

Male euthymic BALB/c-nu mice, aged 4–5 weeks, were purchased from Beijing Vital River Laboratory. All experimental procedures were adhered to the ARRIVE guidelines and received approval from the Ethics Committee of the Institutional Animal Care and Use Committee at Harbin Medical University. Ten mice were randomly assigned to two groups, with five mice in each group (n = 5/group). A549 cells ($6 \times 10^6$ in 200 μL PBS/Matrigel [3:1]) transduced with either a control vector or IRF1 overexpression constructs were injected into the axillary regions of the mice. Tumour volumes were measured with Vernier calipers at seven-day intervals over a period of one month, calculated using the formula ($width^2 \times length$)/2 ($mm^3$), where length (L) represents the longer dimension and width (W) denotes the shorter dimension. The mice were euthanized after 28 days, and tumour tissues were subsequently harvested for further analysis.

### 2.14. Statistical analysis

Data are reported as mean ± SEM from a minimum of three independent experiments for each experimental group. OS and PFS were determined based on the time elapsed from the date of surgery or pathological biopsy to death or relapse, respectively. Survival curves were obtained with the Kaplan–Meier method and assessed with the log-rank test to compare OS and PFS across groups. Log-rank tests were conducted utilizing the survival and survminer packages to assess the effect of IRF1 on OS and PFS, with statistical significance defined as $p < 0.05$. Comprehensive details are provided in the figure legends. Statistical analyses were conducted using R version 4.0.3 and GraphPad Prism software (GraphPad Software Inc., San Diego, CA, USA).

## 3. Results

### 3.1. IRF1 expression analysis in pan-cancer

Initially, RNA sequencing and clinical data from 33 tumour types were obtained from TCGA and GTEx databases. We analyzed the expression of IRF1 and found that IRF1 was upregulated in seven tumours and downregulated in three (Fig. 1A). Low IRF1 expression has been observed in kidney chromophobes (KICH), LUAD, and LUSC. Additionally, IRF1 expression was decreased in adrenocortical carcinoma (ACC), kidney renal papillary cell carcinoma (KIRP), prostate adenocarcinoma (PRAD), thyroid carcinoma (THCA), thymoma (THYM), and uterine carcinosarcoma (UCS) when the analysis was combined with TCGA and GTEx databases (Fig. 1B). Analysis of paired cancerous and adjacent normal tissues revealed consistently low mRNA expression levels of IRF1 across pan-cancer samples

of LUAD and LUSC from TCGA (Fig. 1C). Interestingly, TCGA-based analysis indicated that IRF1 expression varies significantly at different stages of colon adenocarcinoma (COAD), kidney renal clear cell carcinoma (KIRC), KIRP, liver hepatocellular carcinoma (LIHC), pancreatic adenocarcinoma (PAAD), rectal adenocarcinoma (READ), skin cutaneous melanoma (SKCM), testicular germ cell tumours (TGCT) and THCA (Fig. 1D).

### 3.2. Pan-cancer IRF1 expression at the single-cell level

We further investigated the expression of IRF1 at the single-cell level using TISCH2. The analysis revealed elevated IRF1 expression in immune cells across the majority of cancer types, especially in NSCLC, LIHC, and KIRC. This revealed a conspicuous enrichment of IRF1 expression in the malignant cells of stomach adenocarcinoma (STAD) and PRAD (Fig. 1E).

### 3.3. Relationship between IRF1 expression levels and cancer prognosis and diagnosis

The clinical significance of IRF1 across various tumour types was assessed through Kaplan–Meier survival analysis. Elevated IRF1 expression was associated with beneficial OS in LUNG, sarcoma (SARC), and SKCM but had poor OS in KIRP, brain lower-grade glioma (LGG), THYM, and uveal melanoma (UVM) (Fig. 2A).

We also performed ROC analysis to assess the predictive accuracy of IRF1 expression levels in cancerous and normal tissues. The AUC values derived from the ROC analysis for each cancer type are presented. The AUC values indicate that IRF1 expression can reliably differentiate between cancerous and normal tissues across various cancer types, especially cholangiocarcinoma (CHOL) (AUC = 0.829), oesophageal carcinoma (ESCA) (AUC = 0.805), glioblastoma multiforme (GBM) (AUC = 0.927), KICH (AUC = 0.933), KIRC (AUC = 0.835), LUAD (AUC = 0.707), LUSC (AUC = 0.828), PAAD (AUC = 0.754) (Fig. 2B).

### 3.4. Associations of IRF1 expression with TMB, MSI, and immune checkpoint genes in pan-cancer

TMB and MSI are considered critical tumour characteristics and are related to immunotherapy response and prognosis. IRF1 was positively associated with TMB in nine cancers, including bladder urothelial carcinoma (BLCA), COAD, LGG, SARC, and STAD, whereas it was negatively correlated with TMB in ACC, KIRP, TGCT, and THCA (Fig. 3A). This demonstrated that the positive correlations between IRF1 and MSI were significant in COAD and THCA. Additionally, IRF1 negatively correlated with MSI in CHOL, lymphoid neoplasms, diffuse large B-cell lymphoma (DLBC), KIRP, LUSC, ovarian serous cystadenocarcinoma (OV), PAAD, and TGCT (Fig. 3B).

Collectively, IRF1 was upregulated across most immune-infiltration-cell types, including T cells, B cells, etc (Fig. 3C). To assess the influence of IRF1 on the tumour microenvironment, we compared immune cell infiltration between high and low expression groups (Fig. 3D). There was a positive relationship between IRF1 expression and 23 distinct types of immune-infiltrating cells.

### 3.5. Relationship between IRF1 expression and the tumour microenvironment across various cancer types

Stromal and immune cells represent the majority of the tumour-associated normal cells and regulate the growth and progression of malignancy. To evaluate the infiltration of these cells, we employed the ESTIMATE method, which quantifies immune and stromal scores. Our analysis revealed a robust positive correlation between IRF1 expression and the immune score in BLCA, breast invasive carcinoma (BRCA), cervical and endocervical cancers (CESC), COAD, DLBC, ESCA, neck squamous cell carcinoma (HNSC), KICH, KIRC, LGG, LUAD, LUSC, OV, pheochromocytoma and paraganglioma (PCPG), PRAD, SARC, SKSM, TGCT, THCA, UCEC and UVM in TCGA cancers ($R > 0.60$, $p < 2.2e\text{-}16$) (Fig. 4A). Meanwhile, in LUAD, LUSC and so on, we observed a positive association between stromal scores and IRF1 expression ($R \geq 0.30$, $p \leq 7e\text{-}05$) (Fig. 4B).

### 3.6. Association between IRF1 and immune-related genes

Immune-related genes play essential roles in cancer immunotherapy. Immune suppressive, immune activation, MHC, chemokine, and chemokine receptor genes were assembled and analyzed using the Tumour and Immune System Interaction Database (TISIDB). IRF1 expression was positively correlated with most co-inhibitors, co-stimulators, MHC genes, chemokines, and chemokine receptor genes ($p < 0.05$), especially immunostimulatory genes and MHC ($p < 0.01$), in most tumour types (Fig. 5). Some chemokines (including CCL1, CCL2, CCL7, CCL20, CXCL1-3, CXCL5-6, CXCL8, CXCL10-12, CXCL16, and CX3CL1) and chemokine receptors (including CCR1-8, CXCR3-6, and XCL1) are positively associated with IRF1 expression in numerous cancer types. These results indicate a close relationship between IRF1 and the immune microenvironment in cancers; however, further research is needed to elucidate these details.

### 3.7. Correlation between IRF1 and immunoregulatory markers in NSCLC

To elucidate the immunological role of IRF1 in LUAD and LUSC, we examined the correlation between IRF1 expression and genes related to immune infiltration and immune checkpoints. Our findings indicate a significant correlation between IRF1 and a majority of genes related with immune infiltration and immune checkpoint in NSCLC ($p < 0.01$) (Fig. 6). These results suggested that IRF1 plays a fundamental role in NSCLC, particularly concerning its relationship with immune checkpoint-associated genes.

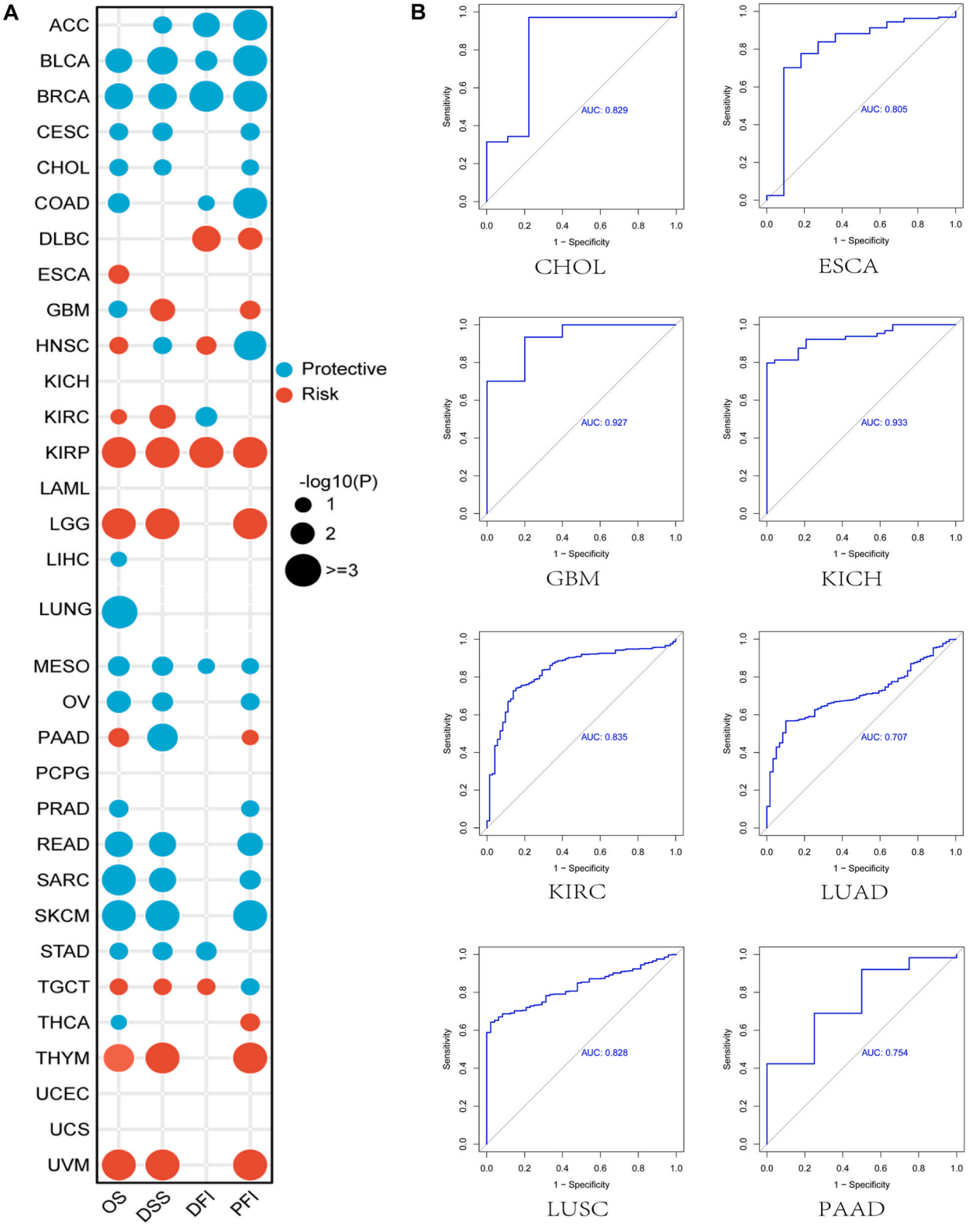


*(caption on next page)*

**Fig. 2.** The relationship between IRF1 expression and cancer prognosis and diagnosis in pan-cancer. (A) The correlation between IRF1 gene expression and survival outcomes was analyzed in 32 distinct tumour types using data from TCGA and the Kaplan–Meier Plotter databases. Survival analyses, including overall survival (OS), disease-specific survival (DSS), disease-free interval (DFI), and progression-free interval (PFI), were conducted using the "survival" and "ggplot2" packages in R software across 33 tumour types. (B) Analysis of specificity and sensitivity of the signature in pan-cancer cohorts with receiver operating characteristic (ROC) based on TCGA. ROC analyses of IRF1 to differentiate patients with malignant tumours from healthy subjects.

### *3.8. Heterogeneity between IRF1-high and IRF1-low cancer cells within lung cancer scRNA-seq datasets*

The association between cell diversity and IRF1 expression in NSCLC was explored at the single-cell level. Single-cell data of the four patients with NSCLC in the GSE117570 database were classified at the first level, as shown in Fig. 7A. According to marker classification, the results showed that myeloid cells were the main type, followed by epithelial and immune cells (NK T and B cells) (Fig. 7B). The reclassification results of the extracted malignant epithelial cells are shown in Fig. 7C, indicating significant heterogeneity of the tumour cells. After classifying them according to IRF1 expression, there were significantly more NSCLC tumour cells with low IRF1 expression than IRF1-high expression group (Fig. 7D). The volcano diagram of the DEGs showed that there were variations in IRF expression, and some other genes also showed differences in expression (Fig. 7E). GO and KEGG database analysis showed that IRF expression is related to the biosynthesis and metabolic regulation of various substances, as well as cellular activity pathways (Fig. 7F and G).

### *3.9. Validation of IRF1 function in LUAD*

We investigated the endogenous expression of IRF1 in both normal lung and cancer cell lines. Our analysis, utilizing qRT-PCR and WB, identified PC9 cells, which exhibit relatively low levels of IRF1, for gain-of-function studies. In contrast, H1993 cells were selected for loss-of-function analysis (Fig. 8A and B).

We then chose the first sequence of siRNA targeting IRF1, which showed the best knockdown effect for subsequent experiments. In addition, cell proliferation declined more significantly in IRF1 overexpression cells than in cells expressing the control vector, as demonstrated by the CCK-8 assay (Fig. 8C). Moreover, Transwell invasion and migration assays demonstrated enhanced invasion and migration of cells knockdown IRF1 (Fig. 8D). Increased IRF1 expression inhibited lung cancer cell migration, as indicated by wound healing assays (Fig. 8E). In contrast, IRF1 knockdown had the opposite effect on cell migration. These results validate the tumour suppressor potential of IRF1 in lung cancer.

### *3.10. IRF1 is correlated with a well prognosis in NSCLC specimens*

We analyzed IRF1 protein expression in LUAD and LUSC tissues to evaluate its clinical significance with immunohistochemical staining on a tissue array comprising 187 samples from patients with NSCLC, including 115 LUAD, 72 LUSC, and 28 normal lung tissue samples. The IHC results indicated that IRF1 was localized in the nuclei of the tumour cells (Fig. 9A and B). Analysis using the KM plotter revealed that patients with elevated IRF1 expression levels exhibited longer PFS ($p = 0.016$) and OS in LUAD tissues ($p = 0.049$) (Fig. 9C). Elevated IRF1 expression in LUSC patients was correlated with a longer PFS ($p = 0.011$) and OS ($p = 0.020$) time compared to those of patients with IRF1-low expression (Fig. 9D). Furthermore, imaging studies demonstrated that levels of IRF1 protein were notably lower in lung adenocarcinoma (LUAD) tissues compared with normal tissues (Fig. 9E). Our findings also indicated that IRF1 expression varied significantly across stages I and IV of LUAD, as well as in stages I and III of LUSC (Fig. 9F).

### *3.11. IRF1 facilitates LUAD progression in vivo*

To investigate the potential role of IRF1 in tumour progression of LUAD *in vivo*, A549 cells were stably transfected with either a control (NC) or an IRF1-overexpression construct using a lentiviral system. These cells were then subcutaneously injected into the right axillary region of nude mice. Tumour growth was monitored over a period of 7–28 days post-implantation, after which the tumours were excised for further analysis. The tumour size exhibited the same trend (Fig. 10A and B). The tumour weight (Fig. 10C) and tumour growth curve (Fig. 10D) were significantly lower in the IRF1-overexpressing group compared to the vector control group. WB results indicated that IRF1 levels were increased in IRF1 xenografts (Fig. 10E). These results further demonstrate that IRF1 inhibits LUAD progression *in vivo*.

## 4. Discussion

To clarify the role of IRF1 in pan-cancer, we performed an extensive analysis of multifaceted information on its expression distribution, clinical prognosis, cancer diagnosis, immune infiltration, and immunoregulation. We found that IRF1 expression was upregulated in most tumours and had good diagnostic and prognostic accuracy for most tumours in TCGA database. The underlying mechanisms of IRF1 in cancers have been previously explored, including macrophage infiltration, tumour progression, and immunotherapy [23,26–28]. Zhou et al. demonstrated that IRF1 expression could serve as a biomarker for CD8 + T-cell infiltration in skin melanoma [29]. IRF1 functions as the primary transcription factor regulating the inducible expression of PD-L1, which regulates

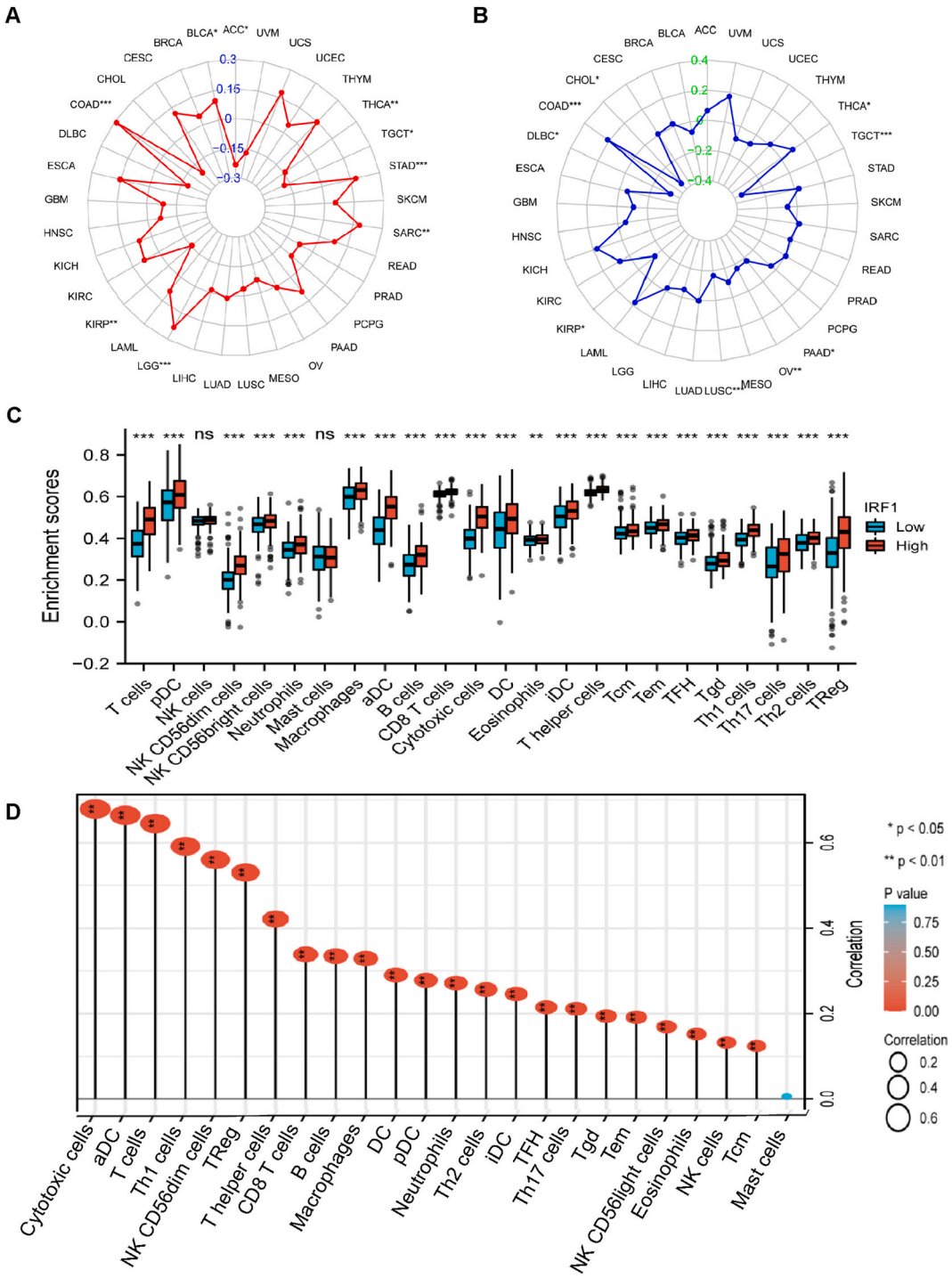


**Fig. 3.** The relationship between IRF1 and immune cell infiltration across various cancers. (A) Radar plot illustrates the correlation between IRF1 and tumor mutation burden (TMB). (B) Radar plot depicts the association between IRF1 expression and microsatellite instability (MSI). (C) IRF1 expression in relation to different types of immune cell infiltration. (D) The comparison of the immune cell infiltration between high-expression and low-expression groups of IRF1.

tumour immune evasion in endometrial cancer [30].

Several studies have indicated that the MSI, TMB, and PD-1/PD-L1 expression levels are strongly associated with competent responses and matched applicability to immunotherapy [31–36]. TMB is recognized as a crucial determinant of the immunogenic neuropeptides displayed on the MHC of the tumour cells, influencing the response to immune checkpoint inhibitors (ICIs) [36], which

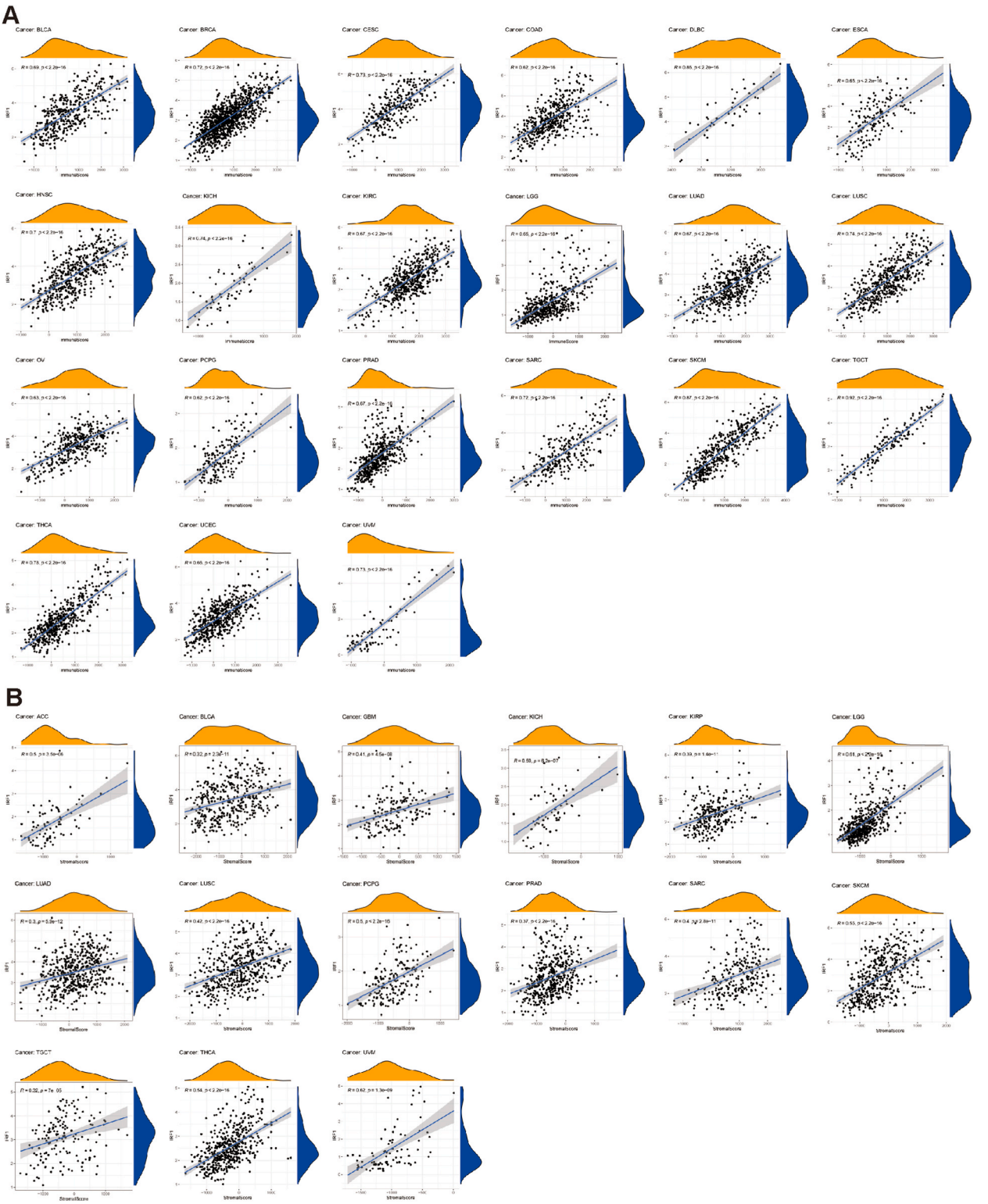


**Fig. 4.** The relationship between IRF1 and ImmuneScore or StromalScore. (A) Correlation of IRF1expression with ImmuneScore in BLCA, BRCA, CESC, COAD, DLBC, ESCA, HNSC, KICH, KIRC, LGG, LUAD, LUSC, OV, PCPG, PRAD, SARC, SKSM, TGCT, THCA, UCEC and UVM. (B) Correlation of IRF1 expression with StromalScore in ACC, BLCA, GBM, KICH, KIRP, LGG, LUAD, LUSC, PCPG, PRAD, SARC, SKCM, TGCT, THCA and UVM.

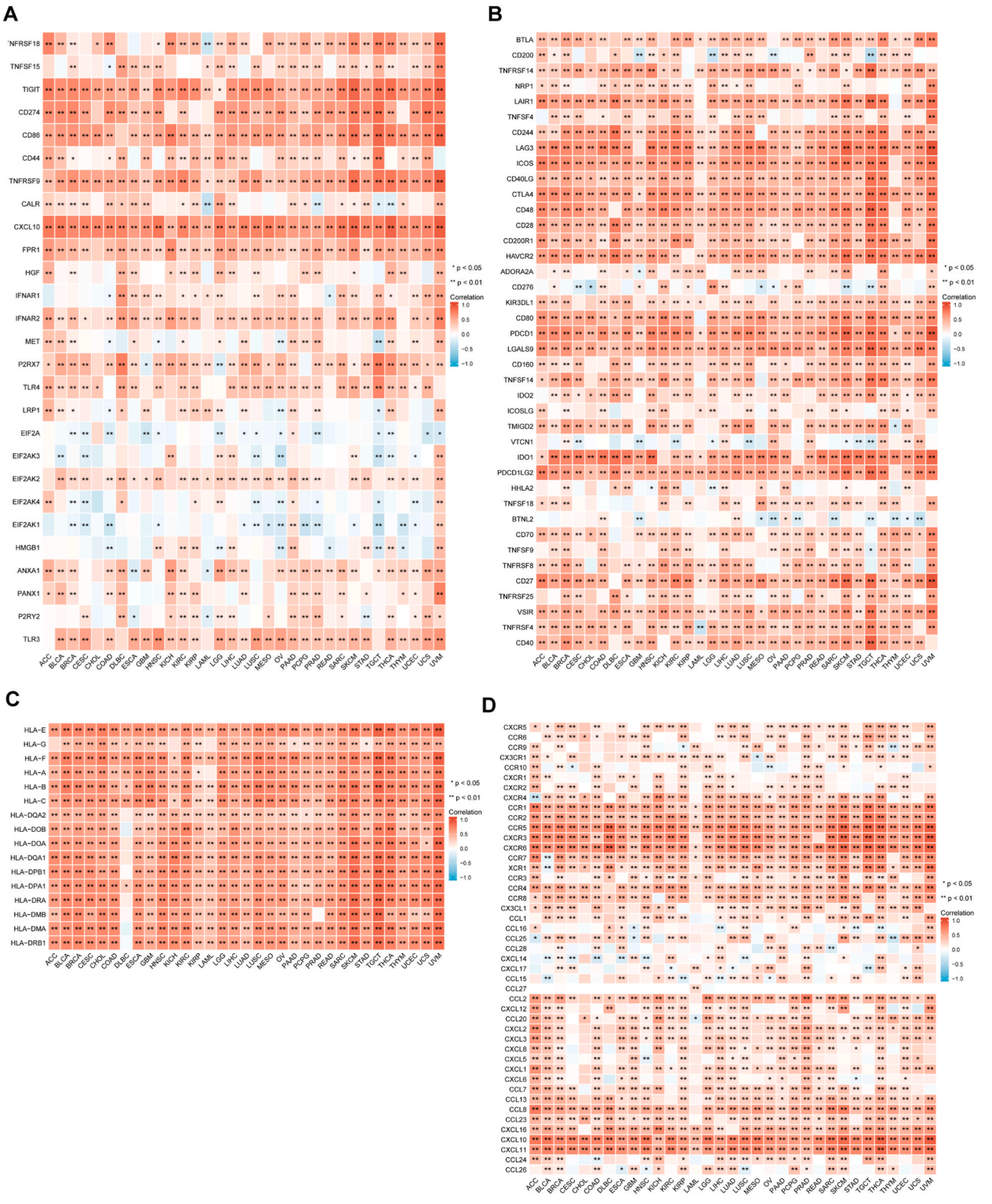


**Fig. 5.** Heatmaps of IRF1 and immune-related gene co-expression. (A) Immune suppressive genes. (B) Immune activation genes. (C) Major histocompatibility complex (MHC) gene. (D) Chemokine and chemokine receptor genes.

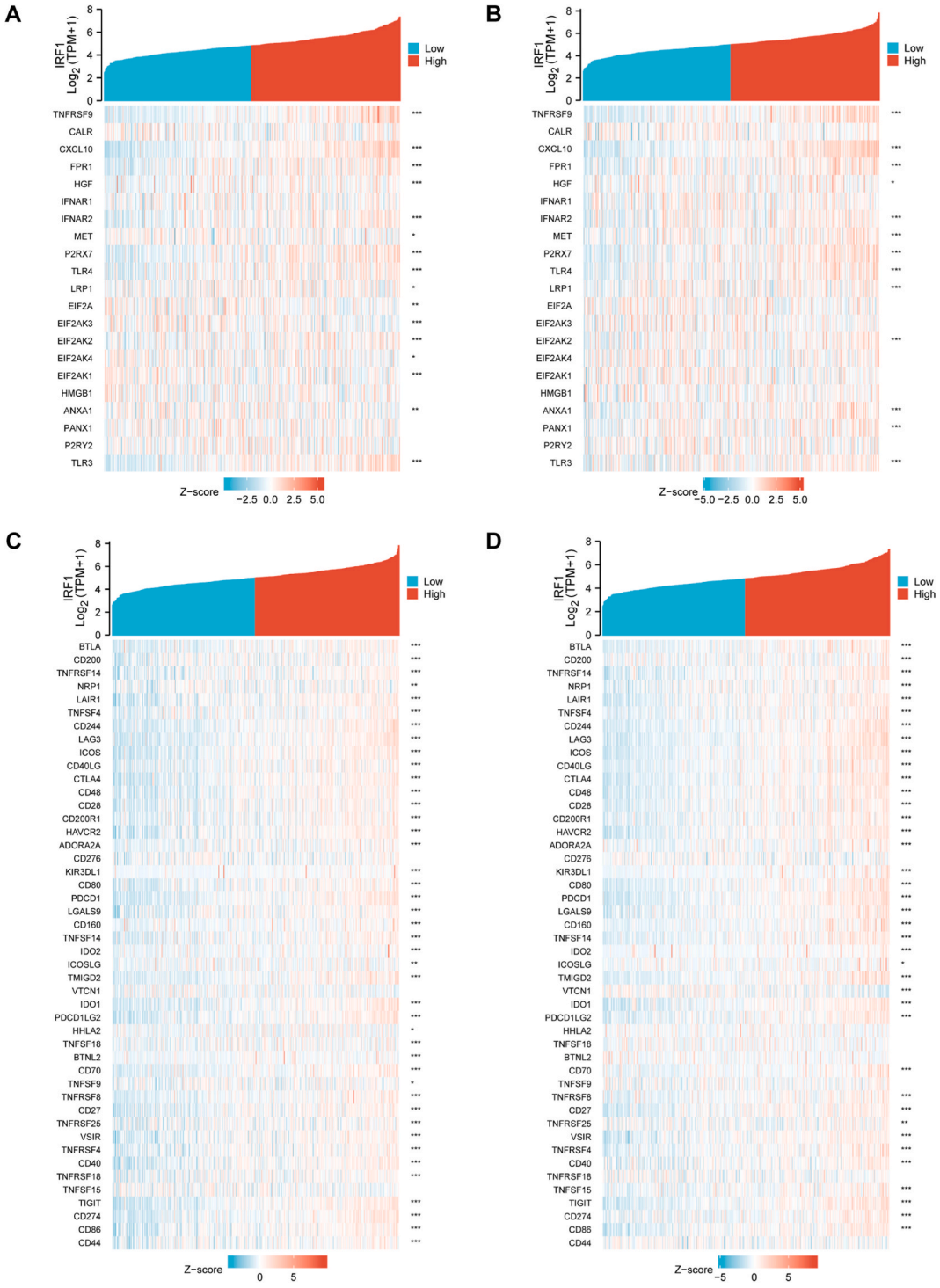


**Fig. 6.** Volcano plots and heatmap of immune-related gene co-expression in non-small cell lung cancer. (A–B) Correlation between IRF1 expression and immune-infiltration-associated genes in LUAD (A) and LUSC (B). (C–D) Correlation between IRF1 expression and immune-checkpoint-associated genes in LUAD (C) and LUSC (D).

are observed in serious solid tumours, including NSCLC, melanoma, and bladder cancer [34]. This may stem from neoantigens and tumour immunogenicity mediated by TMB [32]. Additionally, the classical ICI targets PD-1/PD-L1 and CTLA-4, inhibitors of other ICP genes, such as indoleamine 2,3-dioxygenase (IDO) 1 and T-cell immunoreceptors with Ig and ITIM domains (TIGIT), show correlations

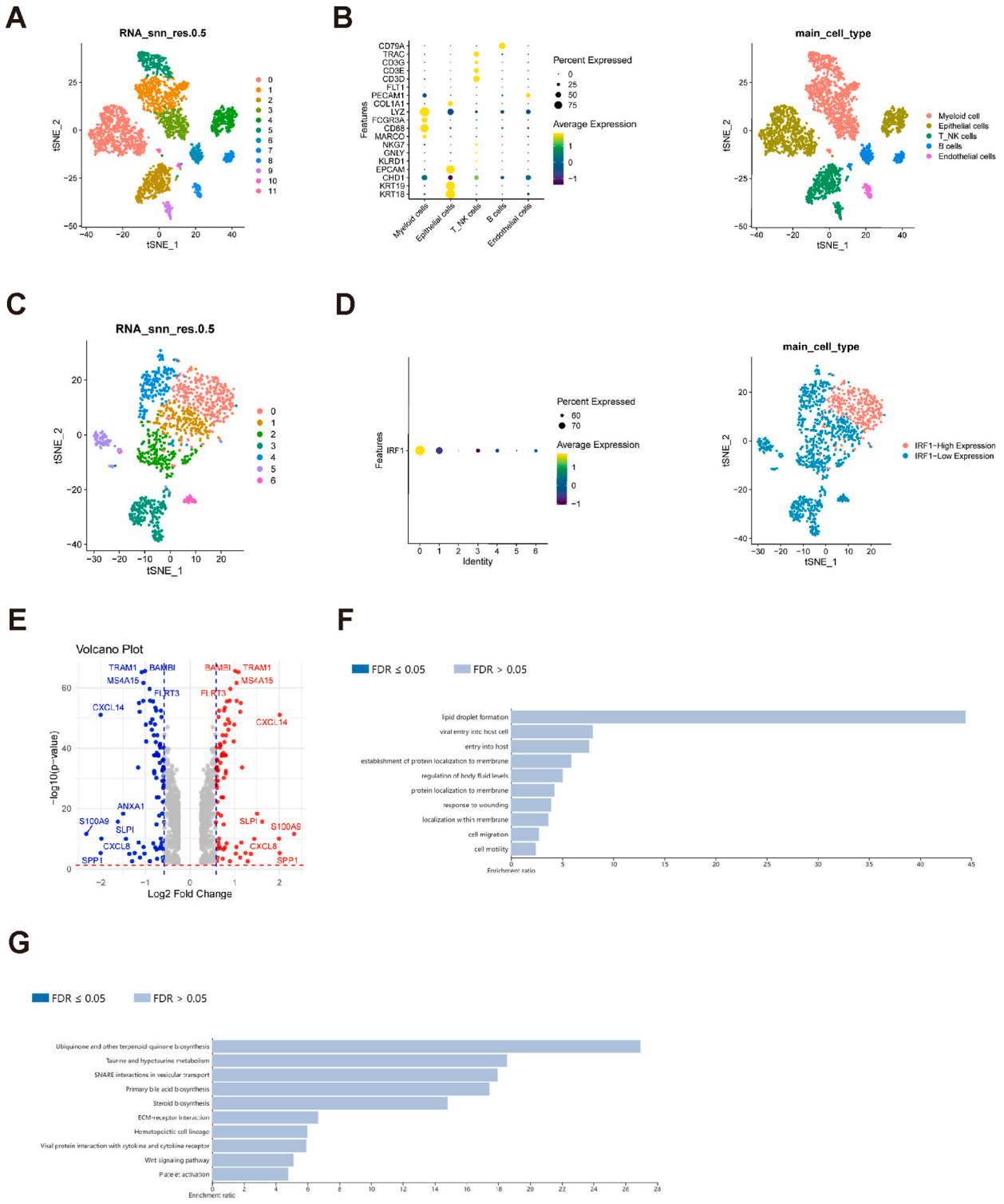


**Fig. 7.** Heterogeneity between IRF1-high and IRF1-low cancer cells within lung cancer scRNA-seq datasets. (A) Primary classification. (B) Determination of cell type based on markers. (C) Extraction of malignant epithelial cells for reclassification. (D) Malignant epithelial cells were categorized into two groups: high-expression and low-expression groups. (E) Differential gene volcano map for differential analysis of high and low-expression groups of IRF1. (F) GO Enrichment analysis of differentially expressed genes through biological processes. (G) KEGG enrichment analysis of differentially expressed genes.

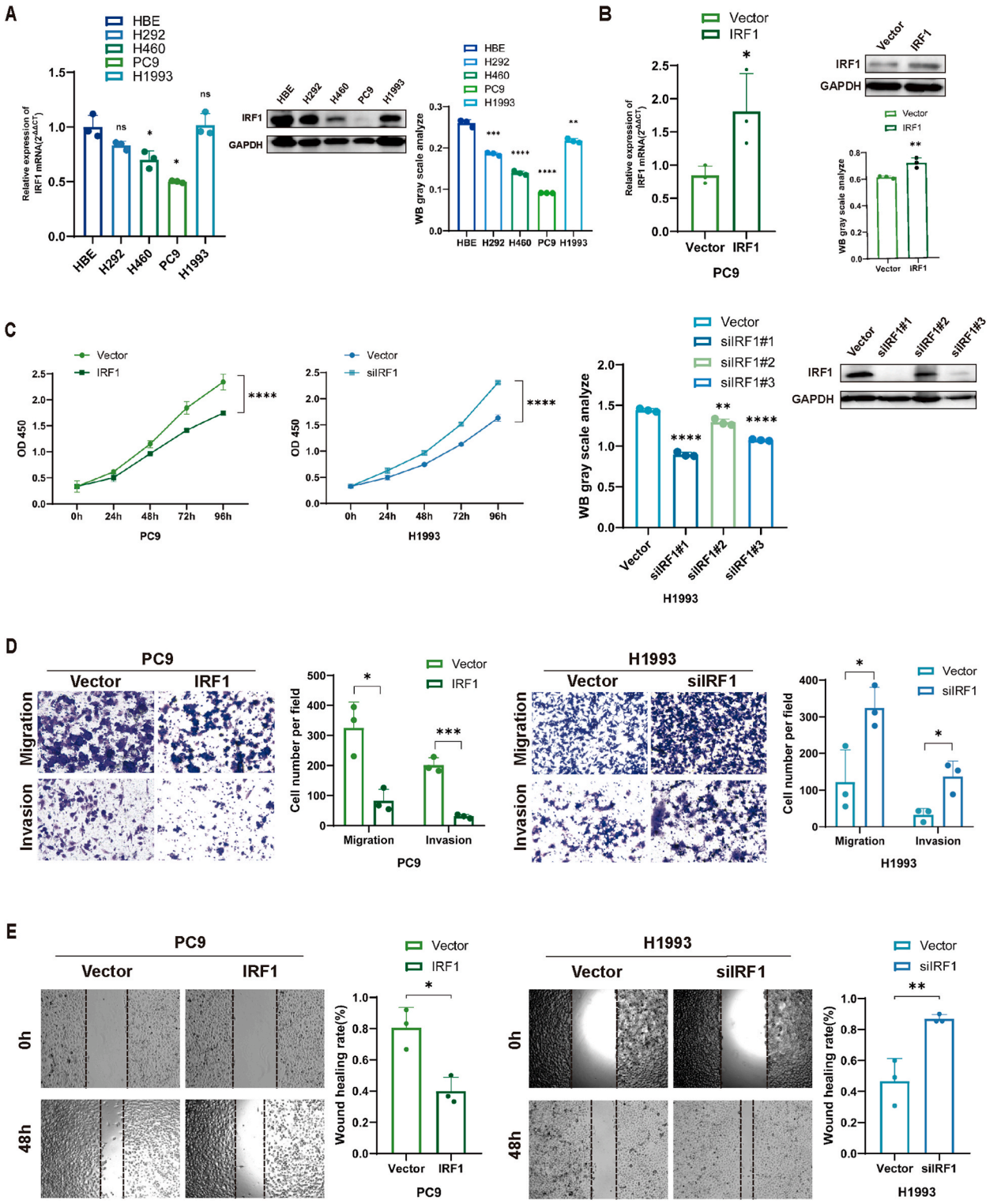


**Fig. 8.** IRF1 inhibited the proliferation and invasion of LUAD cells *in vitro*. (A) The expression levels of IRF1 in HBE and various lung cancer cell lines via qRT-PCR and Western blot. (B) qRT-PCR assays and Western blot were applied to analyse the expression level of IRF1 after transfection by shIRF1 or IRF1 overexpression vector for 48 h in PC9 or 1993 cells. (C) CCK-8 assays. (D) Transwell and Matrigel assays. (E) Scratch assays. Error bars represent the mean ± standard deviation (SD). The complete and unadjusted images of WB can be found in Supplementary Information 1.

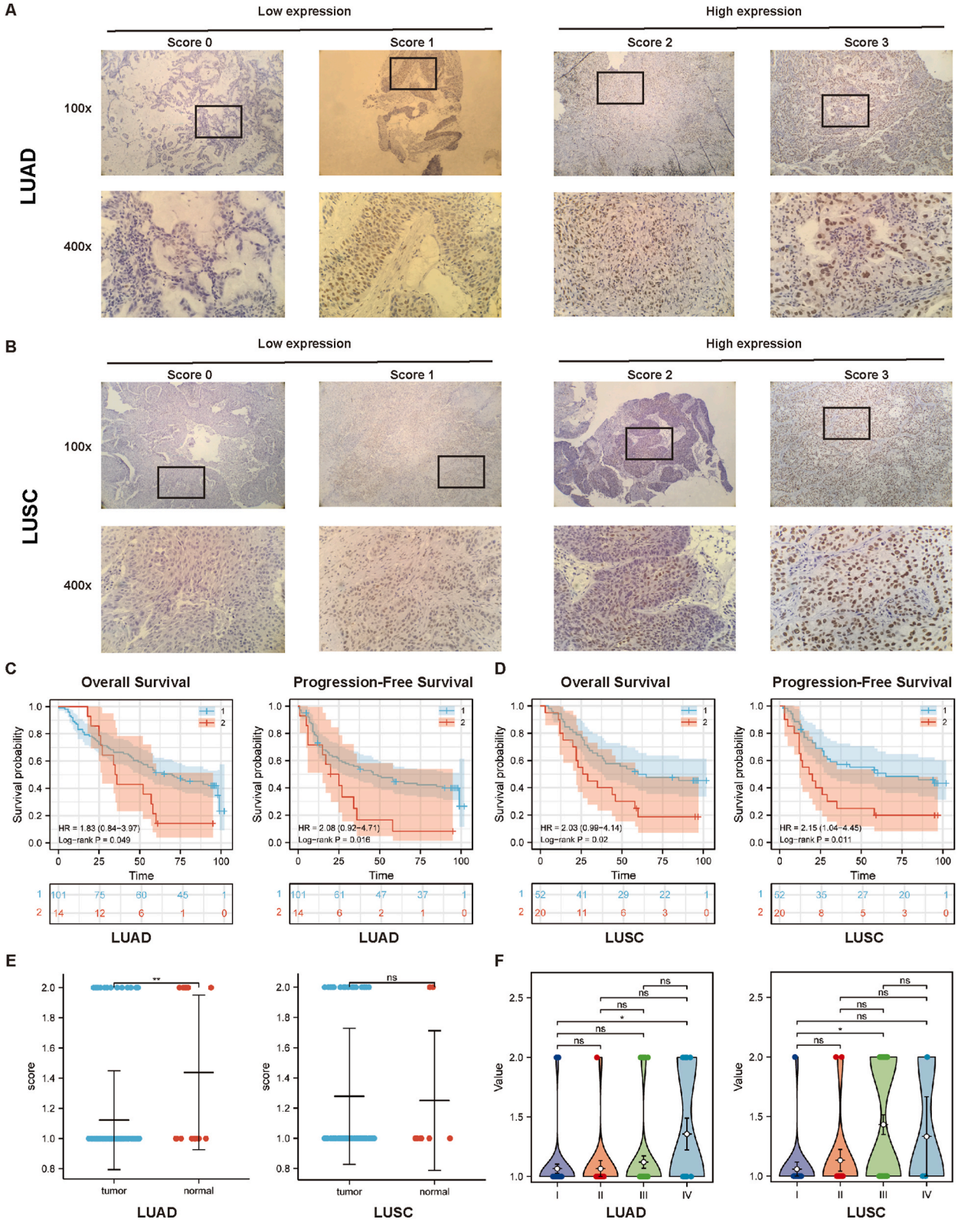


*(caption on next page)*

**Fig. 9.** The association between IRF1 expression and clinical prognosis in NSCLC tissue specimens. (A–B) Representative images of score 0, 1, 2, and 3 staining for IRF1 in clinical LUAD (A) and LUSC. (B) specimens. Magnification, × 100 and × 400. (C–D) The correlations between Kaplan–Meier survival analysis and IRF1 expression level in NSCLC specimens. The correlations of IRF1 expression with the OS and PFS of patients with LUAD (C) and LUSC (D). (E) Box diagram of IRF1 expression between normal and LUAD or LUSC. (F) Violin plot of IRF1 expression among different stages in LUAD or LUSC.

with IRF1 in various tumours [37–39]. Our study produced results that are in agreement with these findings.

The major components of TME are tumour cells, stromal cells—including tumour-associated fibroblasts and endothelial cells—immune cells such as natural killer (NK) cells, T lymphocytes, dendritic cells (DC) and macrophages, as well as the extracellular matrix formed by biochemical components secreted by these cells, alongside blood vessels [40,41]. The TME is important not only for tumour development, including tumour proliferation, invasion, and metastasis but also for immunotherapeutic effects and immunosuppression [42,43]. Zhou et al. found that IRF1 was positively associated with the distribution of the TME in GC [44]. Advances in nanotechnology hold promise for disease prevention, diagnosis, treatment, and monitoring owing to their impact on the TME [45–47]. The ssGSEA was employed to assess the presence of stromal and immune cells in each tumour sample, utilizing RNA sequencing data to derive the "stromal score" and "immune score" [48]. According to major immune coordination patterns, tumours are classified as exhibiting "hot" or "cold" immune patterns, referring respectively to those that are T-cell-infiltrated and inflamed or non-infiltrated and non-inflamed [49]. Furthermore, the "hot" immune pattern of tumours is a better fit for immunotherapy than "cold". The immunophenoscore was utilized to comprehensively evaluate tumour immunogenicity by considering various factors, including MHC molecules, immune checkpoints, immunomodulators, effector cells (such as activated CD8 and CD4 T cells, as well as central memory CD4 and CD8 T cells), and suppressor cells (including regulatory T cells ([Tregs] and myeloid-derived suppressor cells [MDSCs]). This approach enables robust prediction of responses to anti-CTLA-4 and anti-PD-1 therapies [50].

In this study, IRF1 showed reduced expression in tumours and elevated expression in normal tissues, suggesting the presence of tumour suppressor genes in both LUAD and LUSC. The AUC was higher than 0.7 in both LUAD and LUSC indicating a strong diagnostic value. Additionally, IRF1 expression positively correlated with immune scores in both LUAD and LUSC. IRF1 was also associated with most immune infiltration and immune checkpoint-related genes in NSCLC. Single-cell analysis revealed elevated expression of IRF1 in immune cells. In NSCLC cells, there were significantly more cells with low IRF1 expression than with high IRF1 expression. These findings suggest that IRF1 may function as a tumour suppressor gene in NSCLC, mediating its anti-cancer effects through mechanisms related to immune infiltration and associations with immune checkpoint genes. We validated the anti-cancer role of IRF1 in NSCLC through bioinformatics analysis, cellular and patient tissue staining, clinical survival analysis, and animal experiments.

Our findings are largely dependent on online databases, specific algorithms, and programming languages, which may introduce significant heterogeneity and possible effect of bias. Therefore, the results of the bioinformatics analysis cannot be used directly in clinical practice. However, it may provide new treatment, intervention targets, and immunotherapy strategies for patients with tumours. Furthermore, we demonstrated that IRF1 enhances the proliferation, migration, and invasion of NSCLC cells and is related to OS and PFS among patients with LUAD and LUSC.

## 5. Conclusion

In conclusion, our study revealed the critical role of the expression of IRF1 is correlated with clinical prognosis, cancer diagnosis, immune cell infiltration, TMB, and MSI across various cancers. This suggests that IRF1 may function as both an anti-cancer agent and a potential therapeutic target, as well as a valuable prognostic predictor of survival, diagnosis, and immunotherapy in NSCLC, especially in LUAD treatment.

## CRediT authorship contribution statement

**Weiling Sun:** Writing – review & editing, Writing – original draft, Validation, Project administration, Methodology, Funding acquisition, Formal analysis, Data curation, Conceptualization. **Kui Cao:** Writing – review & editing, Writing – original draft, Visualization, Validation, Software, Investigation, Formal analysis, Data curation, Conceptualization. **Siran Wang:** Writing – review & editing, Writing – original draft, Methodology, Formal analysis, Data curation. **Mengdi Lu:** Writing – review & editing, Visualization, Validation. **Jianqun Ma:** Visualization, Validation, Supervision, Formal analysis. **Chunlong Wu:** Visualization, Validation, Supervision, Formal analysis. **Yanbin Zhao:** Project administration, Methodology, Funding acquisition.

## Ethics approval and consent to participate

This study was reviewed and approved by the Ethics Committee of Harbin Medical University with the approval number: No. KY2022-54, dated the 28th of October 2022. All participants provided the written informed consent.

## Data availability statement

All data included in this study are available by contacting the corresponding authors.

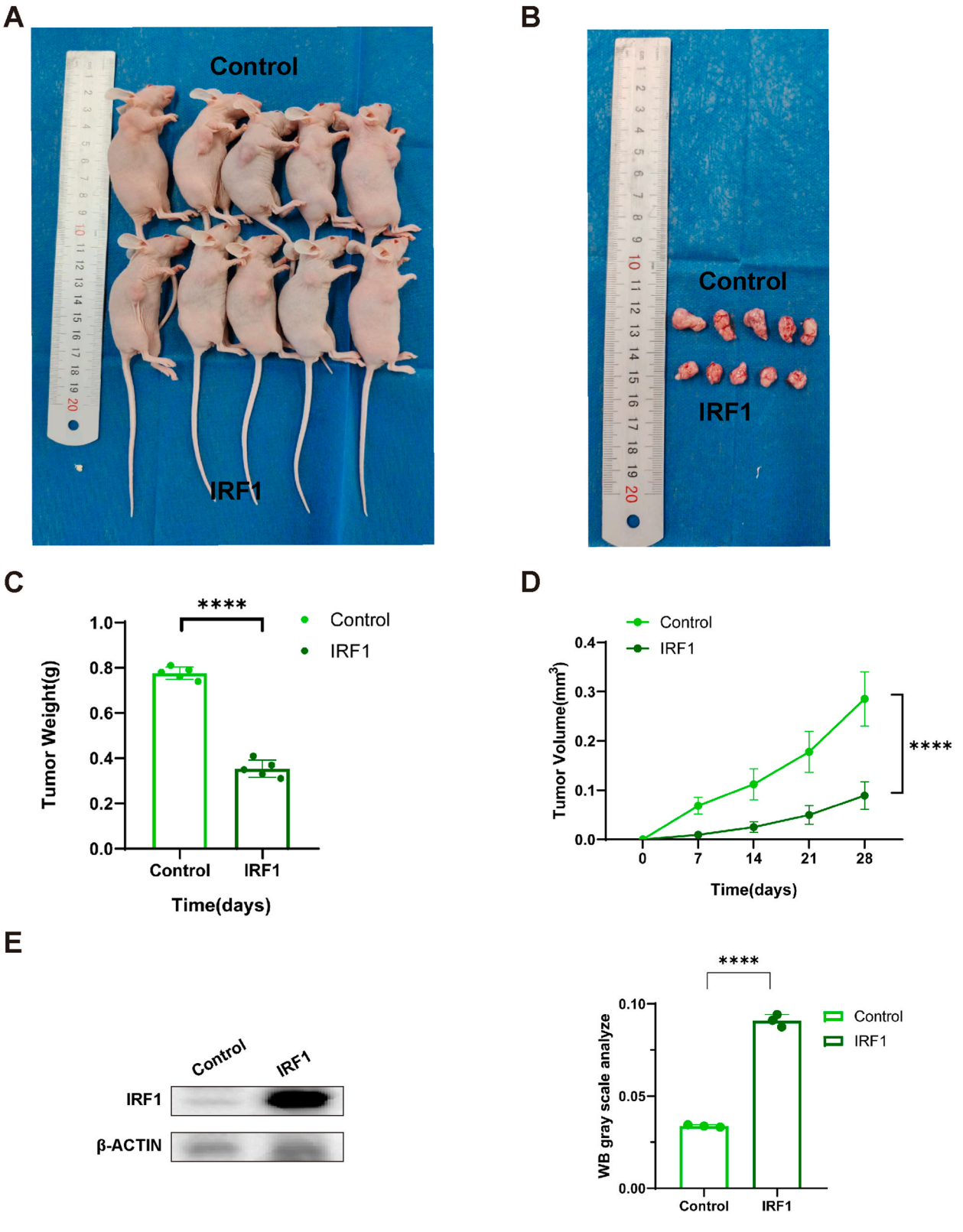


*(caption on next page)*

**Fig. 10.** IRF1 inhibited tumour growth in an orthotopic xenograft model. (A) Mice administrated with vehicle control and IRF1 overexpression. (B) Tumours collected from corresponding mice at 28 days. (C) Tumour weight was measured in the different groups. (D) Tumor volume in nude mice from both groups was measured at 7-day intervals, spanning from day 0 to day 28. (E) Western blotting was employed to assess the protein expression levels of IRF1 in harvested tumour tissues (n = 5 mice in each group). The complete and unadjusted image of WB can be found in Supplementary Information 1.

## Declaration of competing interest

The authors declare the following financial interests/personal relationships which may be considered as potential competing interests: Weiling Sun reports financial support was provided by Heilongjiang Provincial Health Commission. Yanbin Zhao reports financial support was provided by the National Natural Science Foundation of China. Weiling Sun reports a relationship with Heilongjiang Provincial Health Commission that includes: funding grants. Yanbin Zhao reports a relationship with the National Natural Science Foundation of China that includes: funding grants. If there are other authors, they declare that they have no known competing financial interests or personal relationships that could have appeared to influence the work reported in this paper.

## Acknowledgments

This research was funded by Science and Technology Plan Project of Heilongjiang Provincial Health Commission (Grant No. 20230303100250 to W.S.), Haiyan Foundation of Harbin Medical University Cancer Hospital (Grant No. JJZD2023-02 to Y.Z.) and the National Natural Science Foundation of China (81673024 to Y.Z.).

## Appendix A. Supplementary data

Supplementary data to this article can be found online at https://doi.org/10.1016/j.heliyon.2024.e39861.

## References

[1] A. Wang, X. Kang, J. Wang, et al., IFIH1/IRF1/STAT1 promotes sepsis associated inflammatory lung injury via activating macrophage M1 polarization, Int. Immunopharm. 114 (2023) 109478, https://doi.org/10.1016/j.intimp.2022.109478.
[2] H. Feng, Y.B. Zhang, J.F. Gui, et al., Interferon regulatory factor 1 (IRF1) and anti-pathogen innate immune responses, PLoS Pathog. 17 (1) (2021) e1009220, https://doi.org/10.1371/journal.ppat.1009220.
[3] G. Alfarano, M. Audano, P. Di Chiaro, et al., Interferon regulatory factor 1 (IRF1) controls the metabolic programmes of low-grade pancreatic cancer cells, Gut 72 (1) (2023) 109–128, https://doi.org/10.1136/gutjnl-2021-325811.
[4] N. Meyer-Schaller, S. Tiede, R. Ivanek, et al., A dual role of Irf1 in maintaining epithelial identity but also enabling EMT and metastasis formation of breast cancer cells, Oncogene 39 (24) (2020) 4728–4740, https://doi.org/10.1038/s41388-020-1326-0.
[5] B. Wang, H. Yang, L. Shen, et al., Rs56288038 (C/G) in 3'UTR of IRF-1 regulated by MiR-502-5p promotes gastric cancer development, Cell. Physiol. Biochem. 40 (1–2) (2016) 391–399, https://doi.org/10.1159/000452554.
[6] L. Yuan, X. Zhang, K. Cheng, et al., IRF1 inhibits autophagy-mediated proliferation of colorectal cancer via targeting ATG13, Cancer Invest. 40 (1) (2022) 35–45, https://doi.org/10.1080/07357907.2021.1961265.
[7] K.L. Cook, J.L. Schwartz-Roberts, W.T. Baumann, et al., Linking autophagy with inflammation through IRF1 signaling in ER+ breast cancer, Mol Cell Oncol 3 (1) (2016), https://doi.org/10.1080/23723556.2015.1023928.
[8] J. Yuan, Z. Yin, L. Tan, et al., Interferon regulatory factor-1 reverses chemoresistance by downregulating the expression of P-glycoprotein in gastric cancer, Cancer Lett. 457 (2019) 28–39, https://doi.org/10.1016/j.canlet.2019.05.006.
[9] R. Karki, B.R. Sharma, E. Lee, et al., Interferon regulatory factor 1 regulates PANoptosis to prevent colorectal cancer, JCI Insight 5 (12) (2020) e136720, https://doi.org/10.1172/jci.insight.136720.
[10] P. Darvin, S.M. Toor, V. Sasidharan Nair, et al., Immune checkpoint inhibitors: recent progress and potential biomarkers, Exp. Mol. Med. 50 (12) (2018) 1–11, https://doi.org/10.1038/s12276-018-0191-1.
[11] S.R. Gordon, R.L. Maute, B.W. Dulken, et al., PD-1 expression by tumour-associated macrophages inhibits phagocytosis and tumour immunity, Nature 545 (7655) (2017) 495–499, https://doi.org/10.1038/nature22396.
[12] O. Mussafi, J. Mei, W. Mao, et al., Immune checkpoint inhibitors for PD-1/PD-L1 axis in combination with other immunotherapies and targeted therapies for non-small cell lung cancer, Front. Oncol. 12 (2022) 948405, https://doi.org/10.3389/fonc.2022.948405.
[13] X.X. Wang, H. Cao, Y. Zhai, et al., Immune gene signatures and immunotypes in immune microenvironment are associated with glioma prognose, Front. Immunol. 13 (2022) 823910, https://doi.org/10.3389/fimmu.2022.823910.
[14] Y. Wu, L. Zhou, Y. Zou, et al., Disrupting the phase separation of KAT8-IRF1 diminishes PD-L1 expression and promotes antitumor immunity, Nat Cancer 4 (3) (2023) 382–400, https://doi.org/10.1038/s43018-023-00522-1.
[15] L. Shao, W. Hou, N.E. Scharping, et al., IRF1 inhibits antitumor immunity through the upregulation of PD-L1 in the tumor cell, Cancer Immunol. Res. 7 (8) (2019) 1258–1266, https://doi.org/10.1158/2326-6066.
[16] Y. Yan, L. Zheng, Q. Du, et al., Interferon regulatory factor 1 (IRF-1) downregulates Checkpoint kinase 1 (CHK1) through miR-195 to upregulate apoptosis and PD-L1 expression in Hepatocellular carcinoma (HCC) cells, Br. J. Cancer 125 (1) (2021) 101–111, https://doi.org/10.1038/s41416-021-01337-6.
[17] X. Li, J. Huang, Q. Wu, et al., Inhibition of checkpoint kinase 1 (CHK1) upregulates interferon regulatory factor 1 (IRF1) to promote apoptosis and activate antitumor immunity via MICA in hepatocellular carcinoma (HCC), Cancers 15 (3) (2023) 850, https://doi.org/10.3390/cancers15030850.
[18] Y. Yan, L. Zheng, Q. Du, et al., Interferon regulatory factor 1 (IRF-1) and IRF-2 regulate PD-L1 expression in hepatocellular carcinoma (HCC) cells, Cancer Immunol. Immunother. 69 (9) (2020) 1891–1903, https://doi.org/10.1007/s00262-020-02586-9.
[19] A. Bagaev, N. Kotlov, K. Nomie, et al., Conserved pan-cancer microenvironment subtypes predict response to immunotherapy, Cancer Cell 39 (6) (2021) 845–865.e7, https://doi.org/10.1016/j.ccell.2021.04.014.
[20] N.A. Giraldo, R. Sanchez-Salas, J.D. Peske, et al., The clinical role of the TME in solid cancer, Br. J. Cancer 120 (1) (2019) 45–53, https://doi.org/10.1038/s41416-018-0327-z.

[21] M.T. Bilotta, A. Antignani, D.J. Fitzgerald, Managing the TME to improve the efficacy of cancer therapy, Front. Immunol. 13 (2022) 954992, https://doi.org/10.3389/fimmu.2022.954992.
[22] M. Haist, H. Stege, S. Grabbe, et al., The functional crosstalk between myeloid-derived suppressor cells and regulatory T cells within the immunosuppressive tumor microenvironment, Cancers 13 (2) (2021) 210, https://doi.org/10.3390/cancers13020210.
[23] Y. Yan, L. Zheng, Q. Du, et al., Interferon regulatory factor 1(IRF-1) activates anti-tumor immunity via CXCL10/CXCR3 axis in hepatocellular carcinoma (HCC), Cancer Lett. 506 (2021) 95–106, https://doi.org/10.1016/j.canlet.2021.03.002.
[24] C. Li, Z. Tang, W. Zhang, et al., GEPIA2021: integrating multiple deconvolution-based analysis into GEPIA, Nucleic Acids Res. 49 (W1) (2021) W242–W246, https://doi.org/10.1093/nar/gkab418.
[25] D.S. Chandrashekar, S.K. Karthikeyan, P.K. Korla, et al., UALCAN: an update to the integrated cancer data analysis platform, Neoplasia 25 (2022) 18–27, https://doi.org/10.1016/j.neo.2022.01.001.
[26] T. Tamura, H. Yanai, D. Savitsky, et al., The IRF family transcription factors in immunity and oncogenesis, Annu. Rev. Immunol. 26 (2008) 535–584, https://doi.org/10.1146/annurev.immunol.26.021607.090400.
[27] J. Jin, G. Yu, Hypoxic lung cancer cell-derived exosomal miR-21 mediates macrophage M2 polarization and promotes cancer cell proliferation through targeting IRF1, World J. Surg. Oncol. 20 (1) (2022) 241, https://doi.org/10.1186/s12957-022-02706-y.
[28] L.C. Kennedy, J. Lu, S. Kuehn, et al., Liquid biopsy assessment of circulating tumor cell PD-L1 and IRF-1 expression in patients with advanced solid tumors receiving immune checkpoint inhibitor, Target Oncol 17 (3) (2022) 329–341, https://doi.org/10.1007/s11523-022-00891-0.
[29] S. Zhou, C. Lu, G. Liu, et al., IRF1 expression might be a biomarker of CD8+ T cell infiltration in cutaneous melanoma, Expet Rev. Clin. Immunol. 18 (12) (2022) 1319–1327, https://doi.org/10.1080/1744666X.2022.2141228.
[30] K. Gao, Q. Shi, Y. Gu, et al., SPOP mutations promote tumor immune escape in endometrial cancer via the IRF1-PD-L1 axis, Cell Death Differ. 30 (2) (2023) 475–487, https://doi.org/10.1038/s41418-022-01097-7.
[31] A. Marabelle, M. Fakih, J. Lopez, et al., Association of tumour mutational burden with outcomes in patients with advanced solid tumours treated with pembrolizumab: prospective biomarker analysis of the multicohort, open-label, phase 2 KEYNOTE-158 study, Lancet Oncol. 21 (10) (2020) 1353–1365, https://doi.org/10.1016/S1470-2045(20)30445-9.
[32] L. Greillier, P. Tomasini, F. Barlesi, The clinical utility of tumor mutational burden in non-small cell lung cancer, Transl. Lung Cancer Res. 7 (6) (2018) 639–646, https://doi.org/10.21037/tlcr.2018.10.08.
[33] A. Lin, J. Zhang, P. Luo, Crosstalk between the MSI status and tumor microenvironment in colorectal cancer, Front. Immunol. 11 (2020) 2039, https://doi.org/10.3389/fimmu.2020.02039.
[34] T.A. Chan, M. Yarchoan, E. Jaffee, et al., Development of tumor mutation burden as an immunotherapy biomarker: utility for the oncology clinic, Ann. Oncol. 30 (1) (2019) 44–56, https://doi.org/10.1093/annonc/mdy495.
[35] M.G. McNamara, T. Jacobs, A. Lamarca, et al., Impact of high tumor mutational burden in solid tumors and challenges for biomarker application, Cancer Treat Rev. 89 (2020) 102084.
[36] D. Sha, Z. Jin, J. Budczies, et al., Tumor mutational burden as a predictive biomarker in solid tumors, Cancer Discov. 89 (2020) 102084, https://doi.org/10.1016/j.ctrv.2020.102084.
[37] A. Pawlowska, W. Skiba, D. Suszczyk, et al., The dual blockade of the TIGIT and PD-1/PD-L1 pathway as a new hope for ovarian cancer patients, Cancers 14 (23) (2022) 5757, https://doi.org/10.3390/cancers14235757.
[38] Y. Guo, Y. Liu, W. Wu, et al., Indoleamine 2,3-dioxygenase (Ido) inhibitors and their nanomedicines for cancer immunotherapy, Biomaterials 276 (2021) 121018, https://doi.org/10.1016/j.biomaterials.2021.121018.
[39] X. Zhou, S. Khan, D. Huang, et al., V-Set and immunoglobulin domain containing (VSIG) proteins as emerging immune checkpoint targets for cancer immunotherapy, Front. Immunol. 13 (2022) 938470, https://doi.org/10.3389/fimmu.2022.938470.
[40] Y. Dai, C. Xu, X. Sun, et al., Nanoparticle design strategies for enhanced anticancer therapy by exploiting the tumour microenvironment, Chem. Soc. Rev. 46 (12) (2017) 3830–3852, https://doi.org/10.1039/c6cs00592f.
[41] D.C. Hinshaw, L.A. Shevde, The tumor microenvironment innately modulates cancer progression, Cancer Res. 79 (18) (2019) 4557–4566, https://doi.org/10.1158/0008-5472.CAN-18-3962.
[42] K.F. Goliwas, J.S. Deshane, C.A. Elmets, et al., Moving immune therapy forward targeting TME, Physiol. Rev. 101 (2) (2021) 417–425, https://doi.org/10.1152/physrev.00008.2020.
[43] Y. Tang, J. Yuan, Y. Huang, et al., Nomograms for predicting overall survival and cancer-specific survival of patients with stage IV renal cell carcinoma: a SEER population-based study, Nano TransMed 2 (1) (2023) 37–45, https://doi.org/10.26599/NTM.2023.9130014.
[44] H. Zhou, S. Jing, Y. Liu, et al., Identifying the key genes of Epstein–Barr virus-regulated tumour immune microenvironment of gastric carcinomas, Cell Prolif. 56 (2023) e13373, https://doi.org/10.1111/cpr.13373.
[45] H. Wang, W. Ouyang, H. Liu, Tumor microenvironment responsive nanozymes for multimodal imaging of tumors, Nano TransMed (2024) 100032, https://doi.org/10.1016/j.ntm.2024.100032.
[46] P. Ma, G. Wang, K. Men, et al., Advances in clinical application of nanoparticle-based therapy for cancer treatment: a systematic review, Nano TransMed (2024) 100036, https://doi.org/10.1016/j.ntm.2024.100036.
[47] Y. Lu, T. Zeng, H. Zhang, et al., Nano-immunotherapy for lung cancer, Nano TransMed 2 (1) (2023) 7–18, https://doi.org/10.26599/NTM.2023.9130018.
[48] K. Yoshihara, M. Shahmoradgoli, E. Martínez, et al., Inferring tumour purity and stromal and immune cell admixture from expression data, Nat. Commun. 4 (2013) 2612, https://doi.org/10.1038/ncomms3612.
[49] J. Galon, D. Bruni, Approaches to treat immune hot, altered and cold tumours with combination immunotherapies, Nat. Rev. Drug Discov. 18 (3) (2019) 197–218, https://doi.org/10.1038/s41573-018-0007-y.
[50] P. Charoentong, F. Finotello, M. Angelova, et al., Pan-cancer immunogenomic analyses reveal genotype-immunophenotype relationships and predictors of response to checkpoint blockade, Cell Rep. 18 (1) (2017) 248–262, https://doi.org/10.1016/j.celrep.2016.12.019.